Leading- and Trailing-Edge Flaps on a Low Reynolds Number Airfoil

M. L. Perry* and T. J. Mueller†
University of Notre Dame, Notre Dame, Indiana

An experimental study was conducted on a two-dimensional Wortmann FX63-137 airfoil model with a 13%-chord leading-edge flap and a 25%-chord trailing-edge flap at chord Reynolds numbers of 1.0 and 1.5×10^5. Deflecting the leading edge was shown to increase the maximum lift coefficient up to 9.2% while also increasing the maximum l/d. $C_l^{3/2}/C_d$ experienced negligible improvement with leading-edge deflection. A leading-edge droop angle of about 5 deg was found to provide the best performance. Deflecting the trailing edge alone was shown to increase the maximum lift coefficient by up to 14.7%. Deflecting both the leading and trailing edges increased the maximum lift by up to 22.7%. Flow visualization revealed that drooping the leading edge moved the laminar separation bubble slightly downstream. Deflecting the trailing edge downward was shown to shift the line of turbulent separation toward the leading edge.

Nomenclature

C = airfoil chord
C_d = airfoil drag coefficient
C_l = airfoil lift coefficient
$C_{mc/4}$ = airfoil quarter-chord moment coefficient
d = airfoil drag force
D = wing drag force
l = airfoil lift force
L = wing lift force
X = distance from leading edge measured along chordline
α = angle of attack
γ = critical angle, i.e., the angle of attack above which an abrupt decrease in lift takes place

Subscripts

max = maximum value of parameter
min = minimum value of parameter

Introduction

SINCE most flight vehicles operate with a chord Reynolds number above 5.0×10^5, little interest has been shown in the area of low Reynolds number aerodynamics until recently. In the last two decades, the accelerated interest in this area has been due primarily to commercial and military use of remotely piloted vehicles (RPV's). Other examples of low Reynolds number applications include model aircraft, sailplanes, ultralight aircraft, and the inboard sections of propellers, helicopter rotors, and wind turbines. Within these applications there exist several operational conditions that require high aerodynamic efficiency. RPV's, in particular, require wings with high values of L/D and $C_L^{3/2}/C_D$.

The performance of an airfoil section at low Reynolds numbers is critically dependent upon the character of the viscous boundary layer. Important areas of concern are the separated regions, which occur near the leading and/or trailing edges, and transition from laminar to turbulent flow. When the laminar boundary layer separates and transition takes place in the free shear layer, allowing for subsequent reattachment, this region is referred to as a "laminar separation bubble."

The limited amount of research conducted on low Reynolds number airfoils has indicated that airfoil performance may be enhanced by management of the boundary layer: 1) by using leading- and/or trailing-edge devices, 2) by use of surface roughness, or 3) by suction or blowing. Many types of leading- and trailing-edge devices have been studied for high Reynolds number applications. The purpose of leading-edge devices is to increase the camber and, thus, delay leading-edge separation. Both leading- and trailing-edge flaps can serve to increase the camber and, therefore, increase the maximum lift of an airfoil. Deflecting the trailing-edge flap downward at a constant angle of attack almost *always* increases the lift.

Most of the research conducted on leading- and trailing-edge flaps has concentrated on high-chord Reynolds number applications (above 5.0×10^5). Due to the increased interest in efficient low Reynolds number airfoils,[1] it has become necessary to investigate the effects of flaps (both leading- and trailing-edge types) at chord Reynolds numbers below 5.0×10^5. The research described in this paper involved experimentally determining the effects of a drooped leading edge (leading-edge flap) and a plain trailing-edge flap on the performance of a two-dimensional Wortmann FX63-137 airfoil at Reynolds numbers of 1.0 and 1.5×10^5.[2] Due to space limitations, however, only the results obtained at a Reynolds number of 1.5×10^5 will be shown in graphic form. The sign convention for leading-edge droop and trailing-edge flap deflection is shown in Fig. 1.

This study was undertaken to determine if the performance of the Wortmann airfoil could be improved by the addition of leading- and trailing-edge flaps. More specifically, it was hoped that the maximum l/d and $C_l^{3/2}/c_d$ would show significant increases due to changes in the airfoil shape. It was further necessary to conduct this study in order to: 1) broaden the data base regarding the use of leading- and trailing-edge flaps in the low Reynolds number regime, 2) experimentally determine the effects of a drooped leading edge on the performance of an airfoil at low Reynolds numbers, and 3) experimentally determine the effects of a trailing-edge flap on the performance of an airfoil at low Reynolds numbers.

Presented as Paper 86-1787 at the AIAA 4th Applied Aerodynamics Conference, San Diego, CA, June 9–11, 1986; received July 14, 1986; revison received Feb. 14, 1987.

*Graduate Research Assistant, Department of Aerospace and Mechanical Engineering. Currently, Engineer, Lockheed-Georgia Co., Marietta, GA. Member AIAA.

†Professor, Department of Aerospace and Mechanical Engineering. Associate Fellow AIAA.

Experimental Techniques

In order to completely understand the effect of changes in the airfoil geometry on the performance of the Wortmann airfoil, it was necessary to measure the aerodynamic forces as well as to conduct flow-visualization experiments. The three-component strain-gage balance described in Refs. 2 and 3 was used to measure the lift, drag, and pitching moment. Several combinations of leading-edge (0, 5, 10, and 15 deg) and trailing-edge (20, 10, 0, −10, and −20 deg) flap deflection were studied, resulting in a total of 40 conditions. After examining the lift, drag, moment, and drag polar curves, it was decided that flow visualization should be performed with the airfoil's leading edge deflected 5 deg and the trailing-edge flap set at 20, 0, and −20 deg.

The two types of flow visualization utilized in this study were fluorescent minituft visualization[4] and smoke visualization by direct injection.[5] Through the use of smoke visualization, it was possible to determine the approximate location of the laminar separation bubble, more so than with the minitufts. The reverse flow velocities in the bubble region were not sufficient to wiggle the minitufts. However, the minitufts enabled the determination of the turbulent regions (and regions of turbulent separated flow) on the upper surface of the airfoil as well as indicating flow direction.

The two-dimensional model used for this study (Fig. 2) is of the Wortmann FX63-137 cross section, with a 152-mm chord and a 413-mm span. Two-dimensionality was simulated by the use of endplates at either end of the model with end gaps measuring 0.609 mm (0.024 in.). The model was equipped with a drooped leading edge measuring 13% of the chord with a maximum deflection of ±15 deg. The trailing-edge flap measured 25% of the chord with maximum deflections of ±25 deg. Downward deflections are defined as positive. Diagrams of the sting mount force balance and wind tunnel are shown in Figs. 3 and 4. The force and moment measurements were acquired through on-line sampling of the strain-gage voltages. All lift, drag, and quarter-chord moment coefficients presented are corrected values.[2] Reference 6 includes a complete description of the wind-tunnel facilities.

Results

The five parameters used to establish the airfoil performance in this study were the maximum lift coefficient, $C_{l\max}$; the minimum drag coefficient, $C_{d\min}$; maximum, l/d; the quarter-chord pitching moment coefficient, $C_{mc/4}$; and $(C_l^{3/2}/C_d)_{\max}$. Also of interest was the critical angle, defined as that angle above which any increase will result in a large or abrupt change in the performance characteristics. This critical angle is identical in definition to the stall angle for the case of leading-edge stall.

Fig. 1 Definition of leading- and trailing-edge flap deflections.

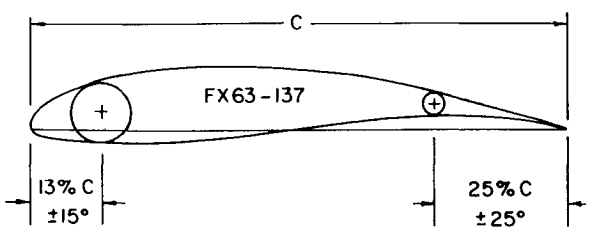

Fig. 2 Wortmann FX 63-137 model with leading- and trailing-edge flaps.

Base Tests

In order to determine the extent to which leading- and trailing-edge deflections influenced the airfoil performance, it was necessary to perform base tests to which all other results could be compared. These base tests were conducted with the flaps undeflected at Reynolds numbers of 1.0 and 1.5×10^5. The results appear in Table 1 and compare favorably with Refs. 3 and 7.

Next, experiments were conducted with the combinations of leading- and trailing-edge flap deflections described earlier at Reynolds numbers of 1.0 and 1.5×10^5. The values of the performance characteristics appear in Table 1, while Table 2 indicates the percentage change in performance parameters compared to the base tests.

Performance as a Function of Leading-Edge Deflection

The overall effect of leading-edge deflection on the lift curve is shown in Fig. 5. For all of the cases, the highest $C_{l\max}$ occurs at a droop angle of 5 deg. In comparison with the baseline cases, it was found that increases in $C_{l\max}$ on the order of 3.3 or 9.2% were realized merely by drooping the leading edge. Also, the highest critical angle for each case occurred at a droop angle of 5 deg. The effect of droop on drag appears in Fig. 6. The effects of droop on the moment coefficient and drap polar are shown in Figs. 7 and 8, respectively. Tables 1 and 2 show that increases in $(l/d)_{\max}$ and $(C_l^{3/2}/C_d)_{\max}$ due to drooping the leading edge are smaller than the uncertainty of the measurements. Therefore, no valid claims of improved performance can be made here.

The continuing reappearance of the 5-deg droop as the best performer prompted the questions regarding an optimum droop angle. The results presented thus far pointed to the 5-deg droop. Further experiments were conducted with 0-deg trailing-edge flap deflection, varying only the droop. Cases for which the leading-edge flap was deflected 6, 5, 4, or 3 deg were studied at a Reynolds number of 1.5×10^5. The 6-deg-droop case yielded the highest $C_{l\max}$, while the 4-deg-droop case resulted in the lowest $C_{d\min}$ and the highest $(l/d)_{\max}$. The highest $(C_l^{3/2}/C_d)_{\max}$ occurred when the leading edge was deflected 3 deg, while deflections of 5 and 6 deg resulted in the highest critical angle. If each of the performance parameters were to be considered equally important, it

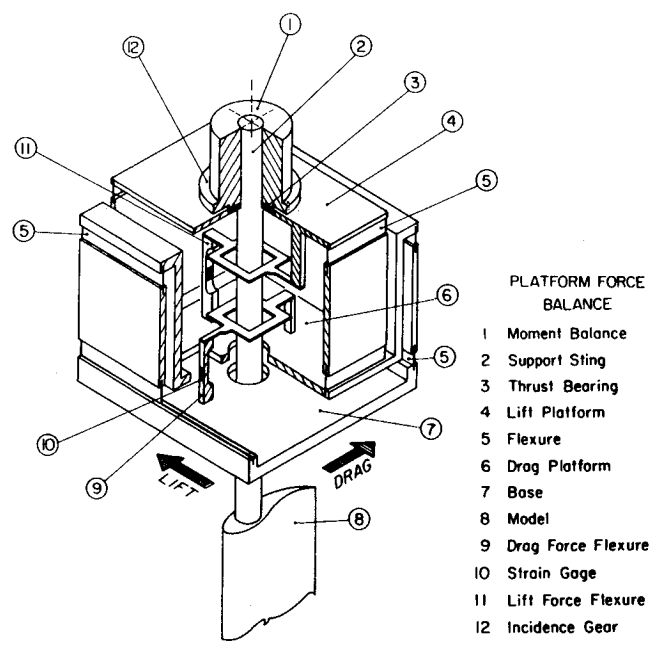

Fig. 3 Force balance apparatus.

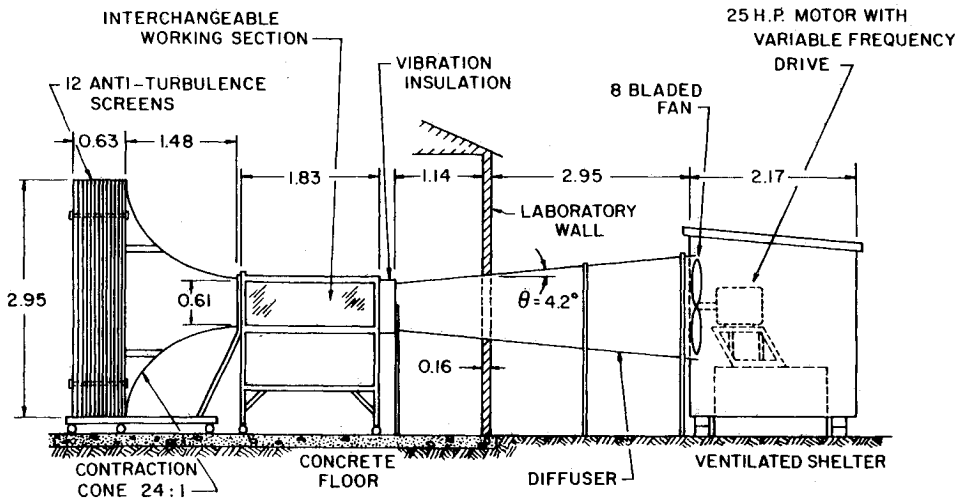

Fig. 4 Low-turbulence subsonic wind tunnel. (All dimensions in meters.)

Table 1 Performance parameters

Droop	Flap	$C_{l\max}$	$C_{d\min}$	$(l/d)_{\max}$	$(C_l^{3/2}/C_d)_{\max}$	Critical angle
			$R_c = 100{,}000$			
0	−20	1.016	0.040	13.36	12.80	18
0	−10	1.304	0.031	16.91	17.47	17
0[a]	0	1.544	0.039	17.55	19.58	16
0	10	1.656	0.061	16.32	19.48	15
0	20	1.748	0.083	12.04	14.81	14
5	−20	0.857	0.041	13.79	11.97	15
5	−10	1.286	0.034	17.96	18.40	14
5	0	1.595	0.044	18.17	19.90	14
5	10	1.769	0.075	16.17	19.24	16
5	20	1.865	0.099	11.86	14.55	17
10	−20	0.960	0.037	13.64	12.21	16
10	−10	1.311	0.039	17.64	17.37	15
10	0	1.536	0.045	17.85	19.13	14
10	10	1.667	0.075	15.98	18.18	13
10	20	1.762	0.112	11.43	13.62	13
15	−20	0.816	0.039	11.87	10.17	15
15	−10	1.205	0.041	17.61	15.51	14
15	0	1.465	0.046	18.16	18.71	14
15	10	1.623	0.070	15.82	17.69	13
15	20	1.714	0.110	11.48	13.25	12
			$R_c = 150{,}000$			
0	−20	1.103	0.036	16.29	15.95	20
0	−10	1.336	0.029	20.98	21.50	19
0[a]	0	1.561	0.031	21.49	23.48	18
0	10	1.680	0.059	19.78	23.77	17
0	20	1.791	0.079	13.82	16.62	16
5	−20	1.247	0.033	15.99	15.44	23
5	−10	1.503	0.030	20.70	20.96	22
5	0	1.705	0.032	21.70	23.73	21
5	10	1.831	0.060	19.23	22.89	20
5	20	1.916	0.093	13.23	15.77	19
10	−20	1.083	0.033	15.40	14.81	17
10	−10	1.384	0.036	18.42	17.41	17
10	0	1.655	0.037	20.97	22.17	16
10	10	1.777	0.058	18.93	21.11	15
10	20	1.868	0.091	12.52	14.33	15
15	−20	1.007	0.035	13.87	13.01	17
15	−10	1.341	0.036	18.72	17.66	16
15	0	1.557	0.042	20.15	20.47	15
15	10	1.695	0.060	18.67	20.58	15
15	20	1.814	0.091	12.57	13.94	14

[a]Indicates baseline test parameters to which all other results are compared in Table 2.

would appear that 4 deg would be the optimum droop angle for this particular airfoil at this Reynolds number.

Performance as a Function of Trailing-Edge Deflection

The general effect of flap deflection on the lift curve appears in Fig. 9. The lift coefficient, in general, is everywhere increased with an increase in flap deflection. The slope of the linear portion of the curve almost always showed some increase as the flap was deflected from 0 to 10 to 20 deg. The postcritical lift coefficient is substantially higher for downward (positive) flap deflections. The effects of flap on drag coefficient, quarter-chord moment coefficient, and drag polar are plotted in Figs. 10–12. The entire moment curve experiences a negative shift as the flap is deflected downward, as may be seen in Fig. 11.

As seen in Tables 1 and 2, the highest value of $(l/d)_{\max}$ occurs at zero flap deflection. It is seen that deflecting the flap does not appreciably increase the value of $(C_l^{3/2}/C_d)_{\max}$, but this, like $(l/d)_{\max}$, is not a great concern. It would appear that optimization of the airfoil's cruise performance can best be achieved by modifying its camber near the leading edge. Maximum lift can be achieved by deflecting both the leading and trailing edges. The cases for a Reynolds number of 1.5×10^5 again show a consistent pattern. As the flap angle is increased, the critical angle decreases. This occurs because as the flap is deflected downward, the point of trailing-edge separation moves forward on the airfoil. This means that trailing-edge separation would reach the leading edge sooner, causing the airfoil to experience the large loss in lift at a lower angle of attack. Also note that the 5-deg-droop case yields the highest critical angle.

Improving Airfoil Performance

As shown in Table 2, the configuration that yielded the highest $C_{l\max}$ for both Reynolds numbers was the case in which the leading-edge flap was drooped 5 deg and the trailing edge was deflected 20 deg. For both Reynolds numbers, minimum drag is achieved with 0-deg leading-edge droop and a −10-deg trailing-edge deflection. The highest $(l/d)_{\max}$ is obtained by deflecting the leading edge to approximately 5 deg with the trailing-edge flap undeflected.

Flow-Visualization Results

After examining the data gathered during force balance testing, it was decided that the 5-deg-droop case should be used for flow visualization, since it usually provided the best performance. The force balance results showed this droop angle to have consistently high critical angles, higher values of $C_{l\max}$, as well as desirable l/d and $(C_l^{3/2}/C_d)_{\max}$ characteristics. It was further decided that flap deflection

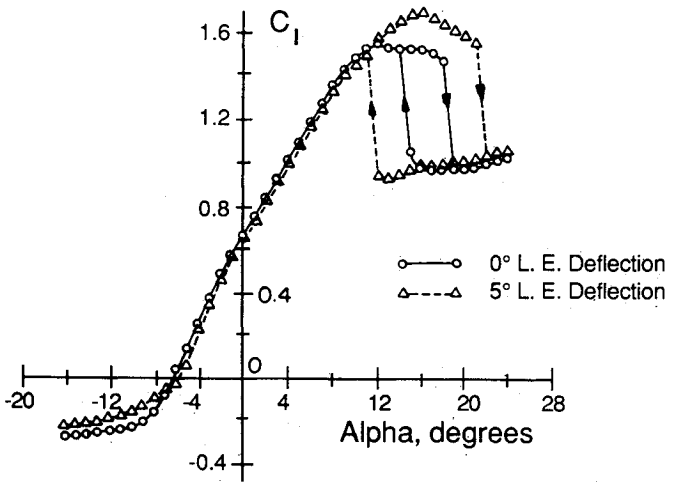

Fig. 5 Overall effect of leading-edge droop on lift coefficient, $R_c = 1.5 \times 10^5$.

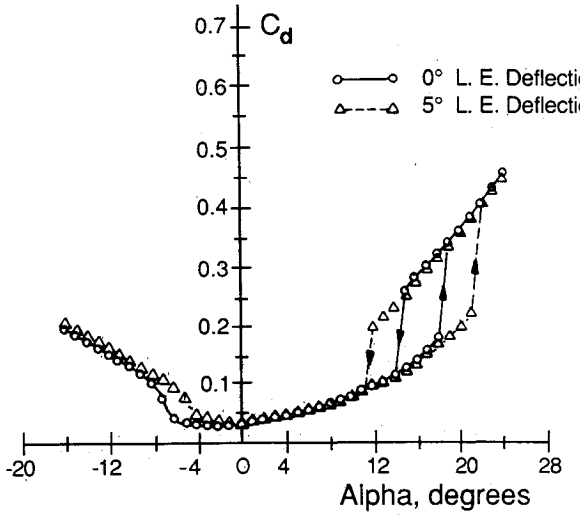

Fig. 6 Overall effect of leading-edge droop on drag coefficient, $R_c = 1.5 \times 10^5$.

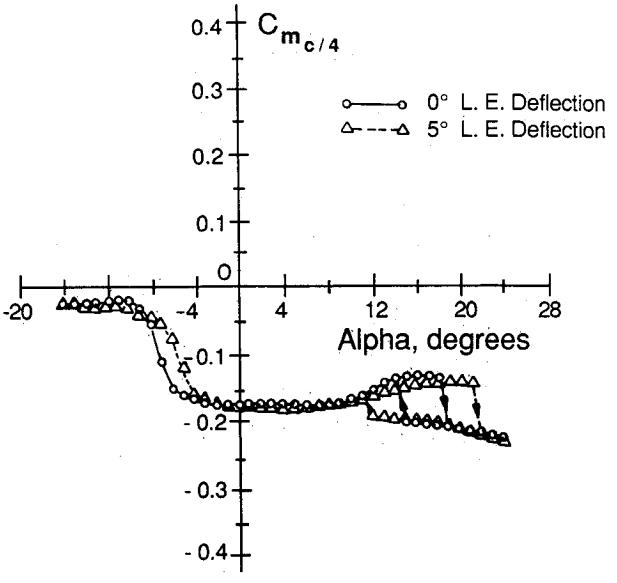

Fig. 7 Overall effect of leading-edge droop on pitching moment coefficient, $R_c = 1.5 \times 10^5$.

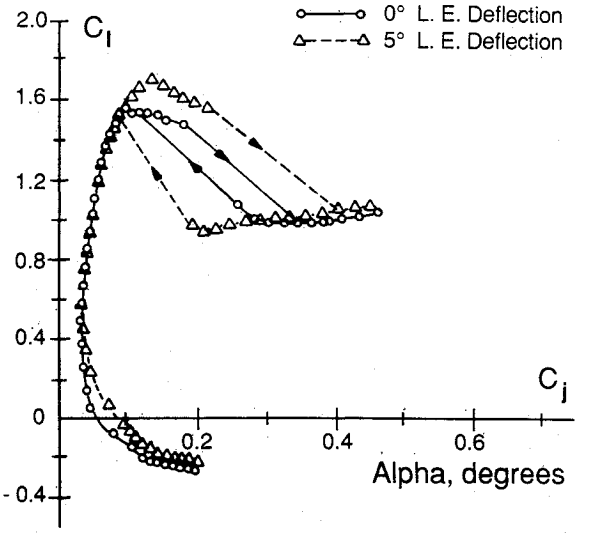

Fig. 8 Overall effect of leading-edge droop on the drag polar, $R_c = 1.5 \times 10^5$.

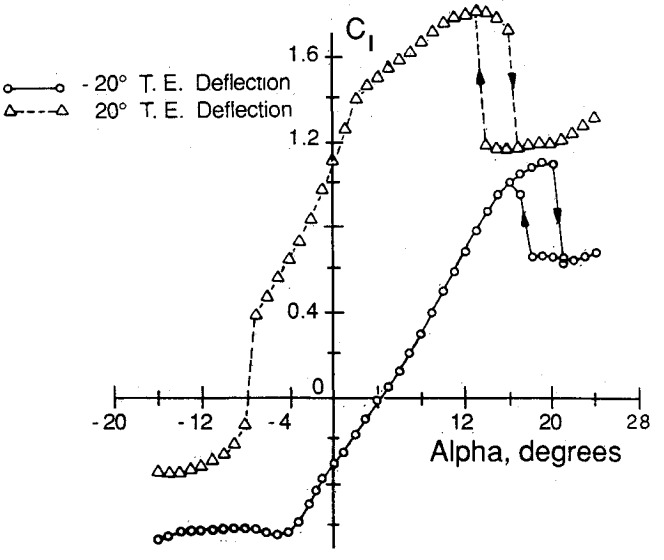

Fig. 9 Overall effect of trailing-edge flap deflection on lift coefficient, $R_c = 1.5 \times 10^5$.

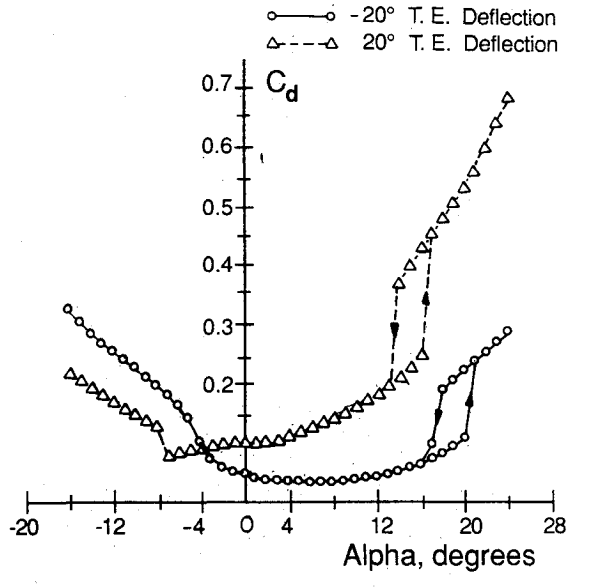

Fig. 10 Overall effect of trailing-edge flap deflection on drag coefficient, $R_c = 1.5 \times 10^5$.

Table 2 Percent change in performance parameters compared to baseline configuration

Test no.	Droop	Flap	$dC_{l\max}$, %	$dC_{d\min}$, %	$d(l/d)_{\max}$, %	$d(En)_{\max}$, %
			$R_c = 100{,}000$			
54	0	−20	−34.2	2.6	−23.9	−34.6
52	0	−10	−15.5	−20.5	−3.6	−10.8
50	0	10	7.3	56.4	−7.0	−0.5
48	0	20	13.2	112.8	−31.4	−24.4
56	5	−20	−44.5	5.1	−21.4	−38.9
58	5	−10	−16.7	−12.8	2.3	−6.0
60	5	0	3.3	12.8	3.5	1.6
62	5	10	14.6	92.3	−7.9	−1.7
64	5	20	20.8	153.8	−32.4	−25.7
66	10	−20	−37.8	−5.1	−22.3	−37.6
67	10	−10	−15.1	0.0	0.5	−11.3
31	10	0	−0.5	15.4	1.7	−2.3
33	10	10	8.0	92.3	−8.9	−7.2
35	10	20	14.1	187.2	−34.9	−30.4
37	15	−20	−47.2	0.0	−32.4	−48.1
39	15	−10	−22.0	5.1	0.3	−20.8
41	15	0	−5.1	17.9	3.5	−4.4
43	15	10	5.1	79.5	−9.9	−9.7
45	15	20	11.0	182.1	−34.6	−32.3
			$R_c = 150{,}000$			
53	0	−20	−29.3	16.1	−24.2	−32.1
51	0	−10	−14.4	−6.5	−2.4	−8.4
49	0	10	7.6	90.3	−8.0	1.2
47	0	20	14.7	154.8	−35.7	−29.2
55	5	−20	−20.1	6.5	−25.6	−34.2
57	5	−10	−3.7	−3.2	−3.7	−10.7
59	5	0	9.2	3.2	1.0	1.1
61	5	10	17.3	93.5	−10.5	−2.5
63	5	20	22.7	200.0	−38.4	−32.8
65	10	−20	−30.6	6.5	−28.3	−36.9
30	10	−10	−11.3	16.1	−14.3	−25.9
32	10	0	6.0	19.4	−2.4	−5.6
34	10	10	13.8	87.1	−11.9	−10.1
36	10	20	19.7	193.5	−41.7	−39.0
38	15	−20	−35.5	12.9	−35.5	−44.6
40	15	−10	−14.1	16.1	−12.9	−24.8
42	15	0	−0.3	35.5	−6.2	−12.8
44	15	10	8.6	93.5	−13.1	−12.4
46	15	20	16.2	193.5	−41.5	−40.6

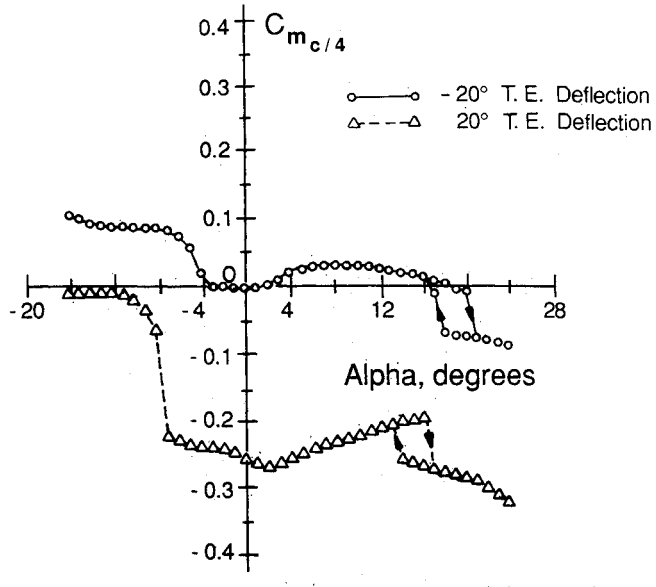

Fig. 11 Overall effect of trailing-edge flap deflection on pitching moment coefficient, $R_c = 1.5 \times 10^5$.

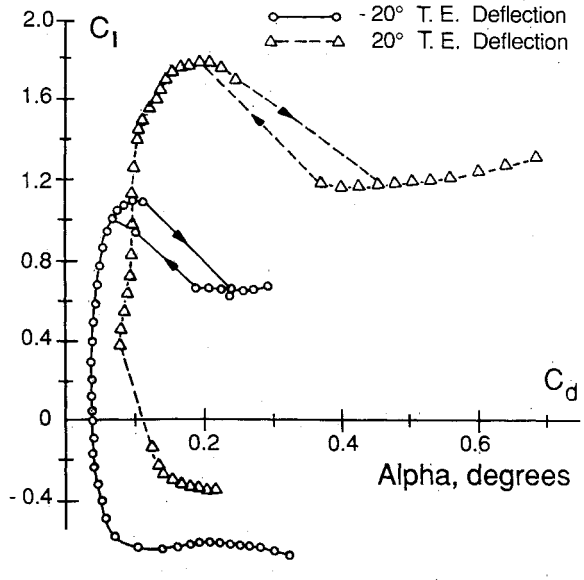

Fig. 12 Overall effect of trailing-edge flap deflection on the drag polar, $R_c = 1.5 \times 10^5$.

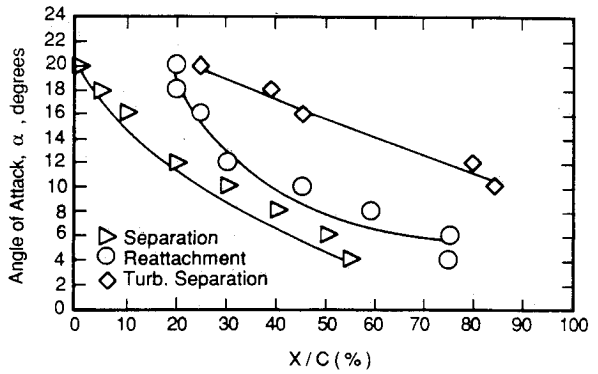

Fig. 13 Separation and reattachment locations, 5-deg leading-edge droop, 0-deg trailing-edge flap deflection, $R_c = 1.5 \times 10^5$.

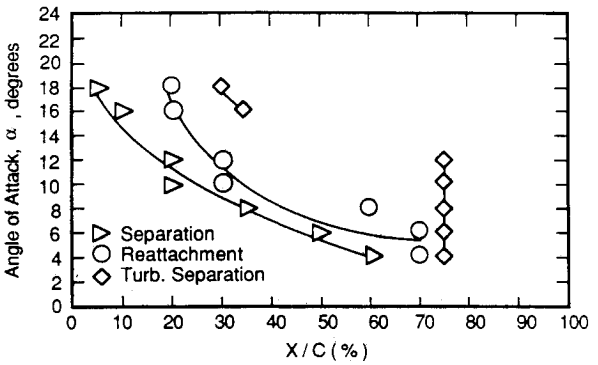

Fig. 14 Separation and reattachment locations, 5-deg leading-edge droop, 20 deg trailing-edge flap deflection, $R_c = 1.5 \times 10^5$.

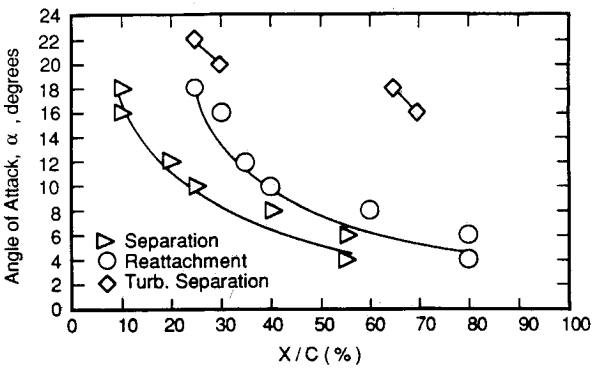

Fig. 15 Separation and reattachment locations, 5-deg leading-edge droop, −20-deg trailing-edge flap deflection, $R_c = 1.5 \times 10^5$.

angles of −20, 0, and 20 deg would provide a representative picture of the flowfield behavior as a function of flap angle.

The two types of visualization techniques used in this study—direct injection of smoke and fluorescent minitufts—yielded two slightly different types of results. Smoke-flow visualization yielded a view of the flow in the plane of the airfoil. This enabled the separation location to be determined. The information obtained, however, was limited to the midspan location where the smoke passed over the airfoil. Therefore, the smoke-flow-visualization experiments gave no indication of the flow at other stations along the span. Earlier experiments had indicated the existence of three-dimensional flow. Minituft visualization, on the other hand, indicated separation on the upper surface over the entire span of the model. From the photographs, it is possible to approximately determine separation, reattachment, and flow direction at any spanwise location. The resolution of the minituft visualization is limited by the size and spacing of the tufts. The size of the tufts is dictated by the requirement that the tuft follows the flow near the airfoil's surface that is related to the stiffness of the tuft and the forces acting upon it. It is felt that the locations of separation and reattachment indicated by the tufts are accurate to within 5% of the airfoil's chord, or approximately half the length of the tufts.

Interpreting the results of flow visualization is not an exact science. It is subject to differing opinions as to where separation, reattachment, etc., occur on an airfoil. If, in this paper, a bubble is not indicated to exist for a certain condition, it does not necessarily mean that a bubble did not occur at that condition. It merely means that the author did not feel there was sufficient evidence to state with any degree of confidence that a bubble did exist.

Photographs were taken of the fluorescent minitufts at a Reynolds number of 1.5×10^5 and angles of attack ranging from −6 to 24 deg. Smoke-flow-visualization photographs were taken at the same Reynolds number, with angles of attack ranging from −12 to 24 deg. The separated region is indicated by the blurring of the tufts in the photographs. If the tufts did not appear blurred in the photographs, it was assumed that the flow was attached and in the direction indicated by the tuft.

From the flow-visualization photographs, the approximate locations of the separation bubble and turbulent separation were determined and are tabulated in Table 3. Plots of these locations as a function of angle of attack appear in Figs. 13-15 for various trailing-edge flap settings. For the two-dimensional case with the leading edge deflected 5 deg, there was considerable movement of the minitufts near the trailing edge (75% chord and rearward) at a −6-deg angle of attack. This movement diminished as the angle of attack increased.

Table 3 Approximate separation points

	Two-dimensional results					
AOA	5 deg 0 deg bubble	Droop flap, TE sep.	5 deg 20 deg bubble	Droop flap, TE sep.	5 deg −20 deg bubble	Droop flap, TE sep.
−6	—	—	—	75	—	—
−2	—	—	—	75	60-80	—
4	55-75	—	60-70	75	55-80	—
6	50-75	—	50-70	75	55-80	—
8	40-60	—	35-60	75	40-60	—
10	30-45	85	20-30	75	25-40	—
12	20-30	80	20-30	75	20-35	—
16	10-25	45	10-20	35	10-30	70
18	5-20	40	5-20	30	10-25	65
20	LE-20	25	Stall	Stall	—	30
22	Stall	Stall	Stall	Stall	—	25
24	Stall	Stall	Stall	Stall	—	—

Note: Figures given are in terms of percentage of chord (X/C) for locations of bubble or trailing-edge separation.

At a 4-deg angle of attack, a separation bubble was detected that extended from approximately 55 to 75% chord and occupied nearly the entire span of the model. As the angle of attack increased, this bubble appeared to migrate forward, and decreased in size until it occupied from 20 to 30% of the chord at a 12-deg angle of attack. At 10 deg, trailing-edge separation appeared with the separation point moving forward as the angle of attack was increased. It should be noted that the trailing-edge separation region is of a cellular nature, longer at midspan and tapering as it approached the ends of the airfoil. As the angle of attack was increased past 20 deg, the trailing-edge separation line reached the leading edge and the stall occurred near 22 deg.

The two-dimensional case with a 5-deg leading-edge droop and a trailing-edge flap deflection of 20 deg shows, in Fig. 14, a massive separation on the upper surface of the flap at all angles of attack. A separation bubble exists on the airfoil at a 4-deg angle of attack from approximately 60 to 70% of the chord, and again at 10 and 12 deg between 20 and 30% of the chord. Trailing-edge separation occurs at the 75%-chord location (the leading edge of the flap) for all angles of attack less than 12 deg, at which point it begins to move forward. By 16 deg, turbulent separation occurs at 35% of the chord. The critical angle occurs near 20 deg.

The dependence of separation location on flap deflection is very simple and straightforward. Trailing-edge flap deflection appears to have very little effect on the location of the separation bubble. Increasing the flap deflection does, however, greatly affect the location of trailing-edge separation. Increasing the flap angle also decreases the critical angle, agreeing with the results of the force balance tests. Flow visualization showed that, for this droop angle, the separation point on the upper surface moved back slightly on the airfoil compared to the undrooped case.

Concluding Remarks

From the large quantity of data collected during this study, several general conclusions may be drawn concerning the effects of leading- and trailing-edge deflection on the performance of this airfoil at low Reynolds numbers.

Drooping the leading edge did not have as large an effect on airfoil performance as deflecting the trailing-edge flap. Drooping the leading edge 5 deg was shown to increase the maximum lift coefficient. A 5-deg droop was also shown to increase the critical angle substantially. This is believed to have occurred because the leading edge would be at an effective angle of attack 5 deg less than the rest of the airfoil. Deflecting the leading edge typically results in a more favorable pressure distribution with lower adverse gradient near the leading edge. Therefore, it is less likely to separate at the leading edge until higher angles of attack are reached. Excessive deflection results in separation near the hingeline. Therefore, an optimum deflection exists.

Flow-visualization results were able to aid in explaining the impact of trailing-edge flap deflection. For example, the maximum lift coefficient increased as the flap was deflected downward. Flow visualization showed that, as the flap deflection was increased, the point of turbulent separation moved forward on the upper surface. This would also indicate that the pressure drag had increased, thereby causing the total drag to increase, which did indeed occur. In fact, the drag for all cases increased by a larger factor than did the lift as the flap was deflected downward. This disproportionate increase in drag was probably the cause of the decrease in $(l/d)_{\max}$ and $(C_l^{3/2}/C_d)_{\max}$ with increasing flap deflections.

Acknowledgments

This research was supported by the Office of Naval Research under Contract N00014-83-K-0239. The authors would like to thank D.R. Bloch, W.D. Michaelsen, and G.S. Schmidt for their comments during the preparation of this manuscript.

References

[1]Mueller, T.J., "Low Reynolds Number Vehicles," AGARDograph 288, Feb. 1985.

[2]Perry, M.L., "The Effects of Leading and Trailing Edge Deflections on the Performance Reynolds Numbers," Master's Thesis, University of Notre Dame, Notre Dame, IN, 1985.

[3]Bastedo, W.G., "Performance of an Airfoil and Three Rectangular Planform Wings at Low Reynolds Numbers," Master's Thesis, University of Notre Dame, Notre Dame, IN, 1984.

[4]Crowder, J.P., "Fluorescent Minitufts for Non-Intrusive Flow Visualization," Douglas Aircraft Co., Paper J7374, 1976.

[5]Mueller, T.J., "Flow Visualization by Direct Injection," *Fluid Mechanics Measurements*, Hemisphere, Washington, DC, 1983, Chap. 7, pp. 301–370.

[6]Brendel, M., Mueller, T.J., and Huber, A.F. II, "The Flow Quality of Subsonic Wind Tunnels with Atmospheric Exhaust," *Journal of Fluids Engineering*, to be published.

[7]Huber, A.F. II, "The Effects of Roughness on an Airfoil at Low Reynolds Numbers," Master's Thesis, University of Notre Dame, Notre Dame, IN, 1985.